Monthly Notices of the ROYAL ASTRONOMICAL SOCIETY **MNRAS Advance Access published December 20, 2013**

MNRAS (2013) doi:10.1093/mnras/stt2261

Early-type stars observed in the ESO UVES Paranal Observatory Project – IV. Studies of CN, CH^+ and CH in the interstellar medium

J. Smoker,[1⋆†] C. Ledoux,[1] E. Jehin,[2] F. P. Keenan,[3] M. Kennedy,[3] R. Cabanac[4] and C. Melo[1]

[1]*European Southern Observatory, Alonso de Cordova 3107, Casilla 19001, Vitacura, Santiago 19, Chile*
[2]*Institut d'Astrophysique et de Géophysique, Université de Liège, B-4000 Liège, Belgium*
[3]*Astrophysics Research Centre, School of Mathematics and Physics, Queen's University Belfast, Belfast BT7 1NN, UK*
[4]*Observatoire Midi-Pyrénées, TBL, 57 Avenue d'Azereix, F-65000 Tarbes, France*

Accepted 2013 November 20. Received 2013 November 20; in original form 2013 February 15

ABSTRACT

High spectral resolution (∼80 000) and signal-to-noise observations from the Ultraviolet and Visual Echelle Spectrograph Paranal Observatory Project (UVES-POP) are used to study the interstellar molecular lines CN (3874 Å), CH^+ (3957, 4232 Å) and CH (3886, 4300 Å) towards 74 O- and B-type stellar sightlines. Additionally, archive data are presented for 140 ELODIE early-type stellar sightlines at $R = 42\,000$, plus 25 FEROS at $R = 48\,000$ and 3 UVES at $R > 50\,000$, mainly in the CH^+ (4232 Å) and CH (3886, 4300 Å) transitions. Detection rates are ∼45 per cent for CN and ∼67 per cent for the other lines in the POP sample, and ∼10–15 per cent for CH^+ and CH lines in the additional sample. CH and CH^+ are well correlated between $\log[N(\mathrm{CH})\,\mathrm{cm}^{-2}]$∼12–14, implying that these clouds are CH^+-like CH and not CN-like CH. CH is also very well correlated with Na I D in the range $\log[N(\mathrm{Na\,I\,cm}^{-2}])$ ∼12.2–14.2. A few sightlines show tentative velocity shifts of ∼2 km s^{-1} between CH and CH^+, which appear to be caused by differences in component strength in blends, and hence do not provide firm evidence for shocks. Finally, we describe a search for $^{13}CH^+$ in a sightline towards HD 76341. No $^{13}CH^+$ is detected, placing a limit on the $^{13}CH^+$ to $^{12}CH^+$ ratio of ∼0.01. If a formal fit is attempted, the equivalent width ratio in the two isotopes is a factor ∼90 but with large errors.

Key words: stars: early-type – ISM: abundances – ISM: clouds – ISM: general – ISM: structure.

1 INTRODUCTION

The ESO Ultraviolet and Visual Echelle Spectrograph Paranal Observatory Project (UVES-POP; Bagnulo et al. 2003)[1] provides a wealth of stellar spectra across the Hertzsprung–Russell Diagram, and spans nearly the entire optical range at a spectral resolution of ∼80 000 (∼3.8 km s^{-1}) and signal-to-noise (S/N) ratios per pixel of many hundreds. The upgraded UVES is described in Dekker et al. (2000) and Smoker et al. (2009). In previous papers, we have used these spectra to study the interstellar medium (ISM), employing O- and B-type stars in the POP Survey as background sources with which to probe interstellar material. These stars are frequently used in ISM studies as they are typically fast rotators and have weak metal and molecular lines (e.g. Mooney et al. 2002, 2004; Smoker et al. 2002, and references therein). Specifically, in Hunter et al. (2006, henceforth Paper I) the interstellar lines of Na I UV ($\lambda_{air} = 3302.368$ Å, 3302.978 Å), Ti II ($\lambda_{air} = 3383.759$ Å) and Ca II ($\lambda_{air} = 3933.661$ Å) were studied towards 74 O- and B-type stars, and basic correlations in the observed column densities investigated. In Smoker et al. (2007, Paper II), we correlated the coordinates of the Paper I sightlines plus additional data with known Intermediate- and High-Velocity Cloud Complexes observed in the 21-cm H I line, to improve the distance limits to a small number of these enigmatic objects. Finally, in Smoker et al. (2011, Paper III), we used UVES-POP observations towards open clusters (IC 2391 and NGC 6475) plus spectra towards Praecepe and archive multi-epoch data to search for variations in the small (pc) and tiny (astronomical unit) scale structure of the ISM in Ti II (3383 Å), Ca II K, Na I D and K I (7698 Å).

Here, we again return to the UVES-POP O- and B-type field star sample, combining this with other observations to investigate the molecular transitions of CN (3874 Å), CH^+ (3957, 4232 Å) and

⋆ E-mail: jsmoker@eso.org
† Based on observations taken at UT2, Kueyen, Cerro Paranal, Chile, ESO DDT programme 265.D-5655(A), UVES Paranal Observatory Project.
[1] See also http://www.sc.eso.org/santiago/uvespop/.

CH (3886, 4300 Å). We only describe the data reduction, analysis and basic correlations between these and Na I (3302 Å, 3303 Å); a subsequent paper will describe in more detail correlations between these molecules and Fe I, Ti II, Ca II and K I, and investigate how elemental ratios change as a function of velocity and column density.

Due to their low dissociation energies, the molecules CN, CH^+ and CH are most frequently found in molecular clouds where dust provides shielding from the ambient radiation field. The current data are generally towards low-reddening objects, in contrast to many previous studies, which until recently had the aim of determining the conditions within normal and high-latitude molecular clouds or star-forming regions (Welty et al. 1989, 2006; Sahu et al. 1998; Pan et al. 2004, 2005; Weselak et al. 2008a,b, 2009). Our spectral resolution of ∼3.8 km s^{-1} is somewhat lower than that of the Pan et al. (2004, 2005) data set (0.6–1.8 km s^{-1}), although with higher S/N ratio (∼400 compared with 50–150). Our POP sample size is comparable to those of previous studies (74 stars compared to, for example, 29 in Pan et al. 2004 or 84 in Weselak et al. 2008a). The additional 168 ELODIE (Moultaka et al. 2004), FEROS (Kaufer et al. 1997) and UVES (Dekker et al. 2000; Smoker et al. 2009) stars add information on some molecules, although typically at lower S/N ratio and spectral resolution than the POP sample.

Section 2 describes our stellar sample, the data analysis and methods used to obtain velocities, velocity dispersions (*b*-values), equivalent widths (EWs) and column densities (*N*) of the molecular lines, including an estimate of the errors in the derived quantities and a comparison with previous results. Section 3 shows the reduced spectra and describes the main results, while Section 4 contains the discussion, and Section 5 the summary and avenues for future research.

2 THE SAMPLE AND BASIC DATA ANALYSIS

Our main stellar sample is described in Paper I, and the analysis of the spectra mirrors that described in the earlier paper, so only brief details are given. The POP subsample used in these papers comprises 74 O- and B-type stars with magnitudes $2.29 < m_v < 7.87$ (median = 6.46) and estimated stellar distances from 62 to 6000 pc (median = 1400 pc). In common with Papers I–III, we used the online reduced versions of the POP Survey data from http://www.eso.org/uvespop, from which we extracted the spectra for the relevant transitions. Additional UVES, FEROS and ELODIE spectra were used to increase the number of sightlines observed, all of which are shown in Table A1 (available online as Supporting Information). Of these, 140 are from ELODIE at a resolution of 42 000, covering CH^+ (4232 Å) and CH (4300 Å) only, 25 from FEROS at a resolution of 48 000 (covering CH^+ at 3957 Å, 4232 Å and CH 3886 Å, 4300 Å), and 3 from UVES with resolutions exceeding 50 000, covering all species in Table 1. The median S/N ratios are ∼150 for the ELODIE spectra, 300 for FEROS and 200 for the extra UVES targets. Note that because the S/N ratios are somewhat lower than for the main POP sample, the detection fraction is much smaller.

Data were converted to ASCII format and read into DIPSO (Howarth et al. 2003) where we normalized the continuum and measured the S/N ratios. Table 1 shows the transitions studied with their air wavelengths and *f*-values. The median S/N ratio per pixel for the POP stars is ∼400 for each of CN (3874 Å), CH^+ (3957, 4232 Å) and CH (3886, 4300 Å), and there are 2 pixels per resolution element. After normalization, the data were shifted to the kinematical local standard of rest (LSR) via the programme RV (Wallace & Clayton 1996). The ELF suite was then used to perform Gaussian fitting to the spectra from which we obtained the EWs, velocity widths and velocity centroids of each of the detected interstellar components. Generally, only a small number of Gaussian components were necessary to provide a good fit. For the UVES-POP sample, we detect CN in 33/73 of the sightlines observed (45 per cent), CH^+ (3957 Å) in 48/73 (66 per cent), CH^+ (4232 Å) in 48/70 (68 per cent), and finally CH (3886, 4300 Å) in 49/72 (68 per cent). The Gaussian fit results were converted to column densities assuming the optically thin approximation and used as initial inputs for the VAPID suite (Howarth et al. 2002) from which we obtained the final column densities, velocities and *b*-values via the creation of model spectra from profile fitting. The VAPID program takes into account optical depth effects. Where more than one line was detected for the same molecule (e.g. 3886 Å and 4300 Å for CH or 3957 Å and 4232 Å for CH^+), a simultaneous fit was undertaken. For CN, we performed a simultaneous fit on the P(1) and R(1) levels. For many components, the observed velocity width was similar to the instrumental resolution of ∼3.8 km s^{-1}; for these components no *b*-value could be determined. Total column densities were estimated by simple summation of the individual profile components. We note that in theory for the $^{12,13}CH^+$ species the situation is not so straightforward, as in both the $^{12,13}CH^+$ 3957 Å and $^{12,13}CH^+$ 4232 Å species the lines are only separated by 0.44 Å and 0.265 Å, respectively, compared with the instrumental resolution of 0.06 Å. However, due to the low $^{13}C/^{12}C$ ratio (Section 4.4) in all sightlines, we can in fact ignore the contribution of the $^{13}CH^+$ component. For the CH lines at 3886 Å and 4300 Å, where a simultaneous fit was obtained, the column density of the 3886 Å line was doubled in order to take into account λ doubling (e.g. Lien 1984).

Table 1. Main transitions studied in this paper. Wavelengths and oscillator strength are from Welty et al. (2006) for all transitions. The derived column density for CH (3886 Å) was doubled due to the fact that this line originates from one of the Λ doubled components.

Species	Transition	λ_{air} (Å)	*f*-value
CN	R(1)	3873.999	0.022 50
CN	R(0)	3874.607	0.033 80
CN	P(1)	3875.760	0.011 40
$^{12}CH^+$	A-X(1-0)	3957.692	0.003 40
$^{13}CH^+$	A-X(1-0)	3958.132	–
$^{13}CH^+$	A-X(0-0)	4232.283	–
$^{12}CH^+$	A-X(0-0)	4232.548	0.005 50
CH	B-X(0-0)	3886.410	0.003 30
CH	A-X(0-0)	4300.313	0.005 06

2.1 Error estimates and comparisons with previous work

In order to obtain the error estimates, we followed a procedure similar to that in Papers I–III. This entailed first obtaining the best fit from VAPID, then creating model fits in which each of the components was varied in *N* and *b*, respectively, by 1, 2, 3, 4, 5, . . . , 98, 99, 100 per cent in turn, the other components being kept fixed at the best-fitting values. Residual data-model spectra were then produced for each of these model fits. When three adjoining bins for the particular component in the residual exceeded 1.0σ,

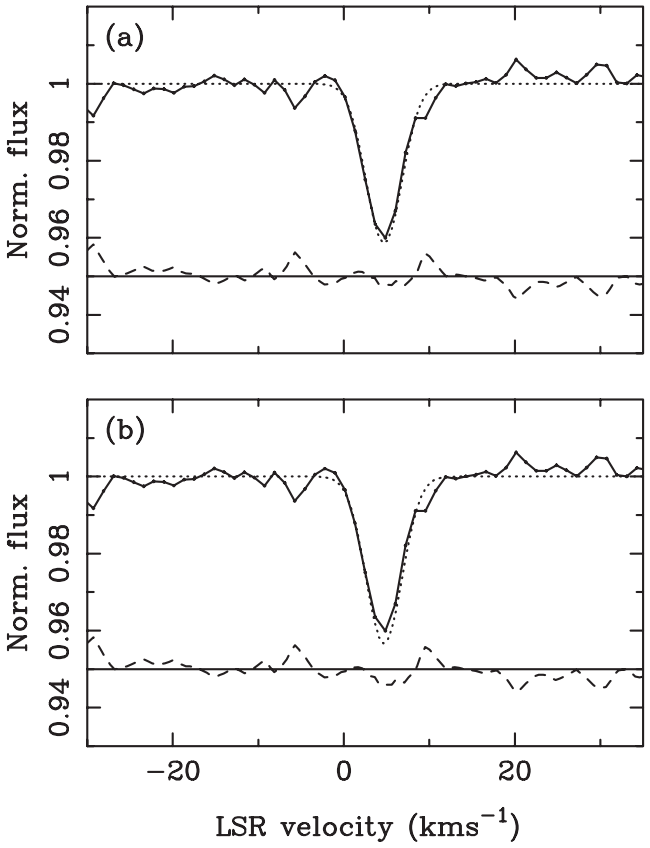

Figure 1. (a) Solid line: CN spectrum of HD 76341. Dotted line: best-fitting component values. Dashed line: Residual data-model fit (offset by 0.95 for display purposes). (b) Corresponding figure for HD 76341 where N was varied by 5 per cent for the component at +5 km s^{-1}. Residual data-model fit (offset by 0.95 for display purposes) in which three adjacent spectral bins around the component have a residual of more than 1.0σ. The final error in N was thus estimated to be 5 per cent.

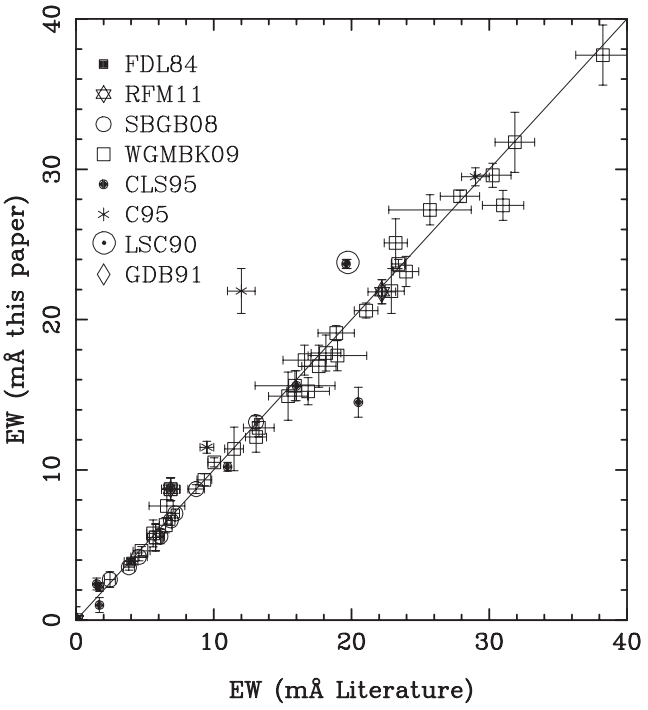

Figure 2. Comparison of the EWs derived in the current paper with literature values. References: CLS95 – Crane, Lambert & Sheffer (1995), C95 – Crawford (1995), FDL84 – Federman, Danks & Lambert (1984), GVB91 – Gredel, van Dishoeck & Black (1991), LSC90 – Lambert, Sheffer & Crane (1990), RFM11 – Ritchey, Federman & Lambert (2011), SGB08 – Slyk et al. (2008), WGMBK09 – Weselak et al. (2009) and references therein.

the difference in N or b between this model and the best fit was taken to be the error for the component. Fig. 1 shows an example of the method used, while Fig. 2 contains comparisons between the EWs derived in the current work with values obtained from the literature. Table A2 (online) shows the comparison with the literature. The agreement is generally acceptable. 1 of the 41 comparison EWs lie outside of the errors. This is HD 115363 which has CH EWs of 31.0 ± 1.5 m Å from Weselak et al. (2009) and 27.6 ± 1.0 m Å (this paper). We have rechecked the fits for our data and find them to be satisfactory. Generally, the good correlation between CH^+ (3957 Å) and CH^+ (4232 Å) also indicates that saturation is unlikely to be an issue for the current sightlines. There are two objects where the derived column densities differ by more than 0.1 dex, being HD 143275 and HD 167264. For the first star, the baseline fit was difficult for the 3957 Å line, and for the second object the 4232 Å line was not symmetric for unknown reasons.

3 RESULTS

3.1 The spectra

Fig. A1 (online) shows the CN (3874 Å), CH^+ (3957, 4232 Å) and/or CH (3886, 4300 Å) spectra towards the 237 sightlines, plotted as normalized flux against LSR velocity. The star name is given in each panel, as well as the Galactic Coordinate. Normally, because the stellar rotational velocities are so high, all but the H I and He I lines are smeared into the continuum. For the $^{12,\,13}CH^+$ data, we note that the velocities of the lines are centred on the $^{12}CH^+$ transition.

3.1.1 Miscellaneous features in the spectra

Several CN (3874 Å) spectra show narrow features shifted by ∼–47 km s^{-1} and ∼+89 km s^{-1} from the main CN line at 3874.607 Å (for example HD numbers 58343, 96917, 112272, 115363 and 136239). These features are simply other CN transitions at λ = 3873.999 Å [R(1)] and 3875.760 Å [P(1)].

Similarly, a number of CH^+ (4232 Å) spectra show narrow features at a rest wavelength of ∼4232.03 Å that are not present in the CH^+ (3957 Å) spectra (for example HD 33328, Be star type B2IVne; HD 49131, Be star type B2III; HD 58978, Be star type B1II; HD 67536, variable star type B2.5Vn; and HD 76131, B6 III). Again, their width is generally narrower than of the stellar sightlines of the main object, although they could be stellar in nature if they come from a spectroscopic companion star. The offset from the main line of ∼–0.52 Å means they are unlikely to be ^{13}CH. Additionally, a number of spectra show stellar lines around CH^+ and CH (e.g. HD numbers 22928, 39985, 42035) that should not be confused with interstellar lines. Examples are shown in Fig. A2 (online).

In HD 37055, variable star type B3IV, and HD 45725, Be star type B3Ve, there are broader absorption-line features in the CH^+ (4232 Å) spectra, but at positive-velocity. Again, the origin of these features could be stellar companions and the lines are not used in the analysis.

Table 2. Component table. See Section 2 for details. The full table is available online in Table A5.

Star	CN				CH+				CH			
	v (km s^{-1})	b (km s^{-1})	log N (cm^{-2}) [R(0)]	log N (cm^{-2}) [R(1),P(1)]	v (km s^{-1})	b (km s^{-1})	log N (cm^{-2})	Line	v (km s^{-1})	b (km s^{-1})	log N (cm^{-2})	Line
HD 886	–	–	–	–	–	–	–	–	5.2 ± 1.5	0.9 ± 10.2	12.04 ± 0.15	B-X
HD 1936	–	–	–	–	-17.0 ± 1.1	8.9 ± 2.0	12.89 ± 0.18	A-X(0-0)	–	–	–	–
HD 3360	–	–	–	–	-131.0 ± 0.3	17.0 ± 2.6	12.71 ± 0.30	A-X(0-0)	–	–	–	–
”	–	–	–	–	20.2 ± 0.3	5.3 ± 2.0	12.45 ± 0.20	A-X(0-0)	–	–	–	–
HD 7636	–	–	–	–	8.3 ± 0.3	4.1 ± 0.6	13.53 ± 0.02	A-X(0-0)	7.1 ± 0.7	2.8 ± 0.4	12.97 ± 0.02	B-X
HD 20809	–	–	–	–	–	–	–	–	-19.3 ± 0.9	0.3 ± 0.0	12.52 ± 0.02	B-X
HD 22951	–	–	–	–	3.8 ± 0.3	2.9 ± 0.4	13.07 ± 0.02	A-X(0-0)	4.6 ± 0.3	1.5 ± 0.2	13.03 ± 0.02	B-X
HD 23302	–	–	–	–	12.1 ± 1.1	0.2 ± 0.0	12.51 ± 0.02	A-X(0-0)	–	–	–	–
HD 23338	–	–	–	–	10.8 ± 0.6	3.0 ± 0.5	12.55 ± 0.02	A-X(0-0)	–	–	–	–
HD 23480	–	–	–	–	13.6 ± 0.3	2.7 ± 0.4	13.26 ± 0.02	A-X(0-0)	11.4 ± 0.3	0.2 ± 86.9	11.82 ± 43.50	B-X
HD 24398	–	–	–	–	4.9 ± 0.5	1.4 ± 0.2	12.52 ± 0.02	A-X(0-0)	5.7 ± 0.3	1.5 ± 0.2	13.34 ± 0.02	B-X
HD 26912	–	–	–	–	16.5 ± 0.3	4.1 ± 0.6	13.14 ± 0.02	A-X(0-0)	15.5 ± 1.0	0.7 ± 0.1	12.48 ± 0.02	B-X
HD 27192	–	–	–	–	2.1 ± 0.3	4.8 ± 0.7	13.24 ± 0.02	A-X(0-0)	3.1 ± 0.3	3.1 ± 0.5	12.95 ± 0.02	B-X
HD 28114	–	–	–	–	47.2 ± 0.5	2.7 ± 0.4	12.92 ± 0.02	A-X(0-0)	46.0 ± 0.3	3.4 ± 0.5	12.97 ± 0.02	B-X
”	–	–	–	–	77.8 ± 0.3	18.2 ± 2.7	13.54 ± 0.10	A-X(0-0)	76.3 ± 1.6	7.3 ± 2.0	12.51 ± 0.22	B-X
HD 29138	–	–	–	–	–	–	–	–	-4.6 ± 1.3	3.4 ± 2.0	12.00 ± 0.23	B-X
”	–	–	–	–	-1.1 ± 0.3	2.5 ± 0.4	12.45 ± 0.04	A-X(0-0, 1-0)	–	–	–	–
”	–	–	–	–	–	–	–	–	2.3 ± 0.9	2.9 ± 1.9	12.04 ± 0.18	B-X
HD 30677	–	–	–	–	8.8 ± 0.3	3.0 ± 0.5	12.38 ± 0.02	A-X(0-0, 1-0)	9.2 ± 0.3	4.0 ± 0.6	12.42 ± 0.03	B-X
HD 32990	–	–	–	–	–	–	–	–	31.7 ± 0.9	4.6 ± 0.7	12.85 ± 0.07	B-X
”	–	–	–	–	34.3 ± 0.5	5.1 ± 0.8	13.31 ± 0.02	A-X(0-0)	–	–	–	–
”	–	–	–	–	137.0 ± 0.6	0.5 ± 0.1	13.00 ± 0.02	A-X(0-0)	–	–	–	–
HD 36861	–	–	–	–	-12.2 ± 0.3	2.8 ± 1.8	11.97 ± 0.17	A-X(0-0, 1-0)	–	–	–	–
”	–	–	–	–	–	–	–	–	10.0 ± 0.3	4.0 ± 0.9	12.39 ± 0.06	B-X A-X
HD 48099	–	–	–	–	28.1 ± 0.3	1.9 ± 1.9	12.53 ± 0.30	A-X(0-0, 1-0)	29.7 ± 0.3	4.1 ± 1.3	12.51 ± 0.11	B-X
”	–	–	–	–	43.9 ± 1.4	4.9 ± 1.5	12.64 ± 0.12	A-X(0-0, 1-0)	43.5 ± 0.3	4.3 ± 1.7	12.53 ± 0.16	B-X
”	–	–	–	–	45.6 ± 0.3	2.3 ± 0.5	12.87 ± 0.04	A-X(0-0, 1-0)	–	–	–	–
HD 49131	–	–	–	–	–	–	–	–	-1.4 ± 0.3	0.5 ± 0.1	11.55 ± 0.02	B-X
HD 58343	-1.1 ± 2.7	0.2 ± 0.2	11.28 ± 0.20	10.58 ± 0.86	1.4 ± 0.3	3.8 ± 0.6	13.01 ± 0.06	A-X(0-0, 1-0)	–	–	–	–
”	–	–	–	–	–	–	–	–	1.6 ± 0.3	3.5 ± 0.6	12.56 ± 0.05	B-X
HD 67536	–	–	–	–	0.9 ± 0.3	2.3 ± 0.4	12.38 ± 0.05	A-X(0-0, 1-0)	0.6 ± 0.3	4.4 ± 1.2	12.22 ± 0.10	B-X
HD 68761	0.4 ± 0.3	1.4 ± 0.9	11.64 ± 0.06	11.18 ± 0.24	0.4 ± 0.3	2.5 ± 0.6	12.56 ± 0.06	A-X(0-0, 1-0)	0.3 ± 0.3	1.9 ± 0.3	12.91 ± 0.02	B-X
”	–	–	–	–	6.0 ± 1.1	0.2 ± 0.2	11.75 ± 0.20	A-X(0-0, 1-0)	–	–	–	–
”	–	–	–	–	10.2 ± 0.3	1.2 ± 1.2	12.21 ± 0.06	A-X(0-0, 1-0)	9.3 ± 0.9	6.5 ± 1.6	12.30 ± 0.10	B-X
”	–	–	–	–	13.6 ± 8.5	7.2 ± 2.0	12.06 ± 0.23	A-X(0-0, 1-0)	–	–	–	–

3.2 Stars not used in the analysis or with uncertain fits

A number of stars were not used in the final analysis, generally because of contamination by stellar lines. These are listed in Table A3 (online). Table A4 (online) summarizes the final list of stars used and detections.

3.3 Tables of profile fits and total column densities

Table 2 shows the results of profile fitting to the individual components for a subset of the sample, with Table A5 (online) showing the whole sample. Listed are the star names, and for each component the velocity in km s^{-1}, *b*-value in km s^{-1} and the log of the column density in cm^{-2} for CN, CH^+ and CH, respectively. We show results for both CN (λ3873.99 Å plus λ3875.76 Å, simultaneously fitted) and CN (λ3874.61 Å). Components were initially associated if they lie within 2.5 km s^{-1} in velocity. A number of components in different lines that fall just outside of the 2.5 km s^{-1} limit were then associated by hand, for example HD 58343 at $v = 0$ km s^{-1}. Table 3 lists the total column densities (derived by summation of the individual components) for a subset of the sample, with the whole of the sample listed in Table A6 (online), or 3σ upper limits only, plus the S/N ratios for each sightline and derived CN excitation temperature T_{ex}. This is governed by the Bultmann equation which simplifies to $T_{ex} = 5.442/\ln[3N(0)/N(1)]$, where $N(1)$ is the column density derived from [R(1)] and [P(1)] and $N(0)$ that derived from [R(0)] (e.g. Pan et al. 2005; Ritchey et al. 2011).

For all sightlines excepting HD 58343, the derived excitation temperatures are in the range from 2.5 ± 0.3 to 3.8 ± 0.9 K. The value for HD 58343 is 1.7 ± 0.7 K although the CN lines are very weak [no CN (3875.76 Å) line detected] and the derived temperature is thus uncertain. Hence, in common with Pan et al. (2005b) and Ritchey et al. (2011), these values are consistent with no great extra excitation in addition to that due to the cosmic microwave background.

4 DISCUSSION

As in Paper I, in this section we search for correlations between the total column densities, and column density ratios, with each other. The derived correlations shown in Table 4 were obtained using the ASURV package (Lavalley, Isobe & Feigelson 1992) and were analysed using the Buckley–James and generalized Kendalls Tau methods, that allow upper limits to be taken into account.

Table 4. Result of fits comparing the total column densities using ASURV which takes the upper limits into account. Both the linear regression by Buckley–James method and a correlation test using generalized Kendalls Tau are presented. In all cases, the probability that a correlation is not present is equal to 0.00.

Variable *y*	Variable *x*	Intercept (lin. reg.)	Gradient (lin. reg.)	Corr. Coeff. Tau
H I	CH	−23.3	1.71 ± 0.45	0.53
H I	CH^+	−32.2	2.13 ± 0.41	0.64
H I	CN	−52.0	2.99 ± 1.14	0.45
CN	CH^+	−5.2	1.26 ± 0.37	0.35
CN	CH	−10.2	1.65 ± 0.21	0.63
CN	Na I	−12.7	1.76 ± 0.23	0.65
CH^+	CH	1.4	0.90 ± 0.05	0.64
Na I	CH^+	2.1	0.81 ± 0.10	0.35
Na I	CH	−0.1	0.96 ± 0.05	0.58

Additionally, we discuss differences in *b*-values of components of different molecules and the velocities of CH and CH^+ in order to find evidence for shocks. Finally, one sightline of high CH^+ column density is searched to determine the $^{13}CH^+$ to $^{12}CH^+$ ratio.

4.1 Correlations of column density with H I column density

4.1.1 Correlations with H I column density

Fig. 3 shows plots of the total column density in each of the observed species against that for H I, taken from Lyα absorption line measurements (see Paper I). Federman (1982) and Weselak et al (2008a) find that there is a large scatter between the column density of CH^+ and molecular, atomic and total hydrogen, and hence suggest that there is no relation between the abundances of methylidyne and hydrogen. The range in log[N(H I) cm^{-2}] column density studied was from ∼20.30 to 21.60. This is in contrast to the literature plus submm study of Falgarone, Phillips & Pearson (2005) who found a good correlation between CH^+ and (H I+H_2). The current observations also show reasonable correlations, with the range in log[N(H I) cm^{-2}] column density studied from 20.2 to 21.6 being similar to that of Weselak et al. (2008a). The correlation coefficient

Table 3. Total column densities (or upper limits) and S/N ratios for CN, CH^+ and CH (4300) for a subset of the sample. The full table is available online in Table A6.

Object	log$N$(CN) (cm^{-2}) [R(0)]	log$N$(CN) (cm^{-2}) [R(1),P(1)] simul	T_{ex} (K)	log$N$(CH^+) (cm^{-2})	CH^+ trans. used	log$N$(CH) (cm^{-2})	CH trans. used
HD 886	–	–	–	<11.88	A-X (0,0)	<11.87	A-X
HD 929	11.69 ± 0.02	–	–	<13.00	A-X (0,0)	<13.00	A-X
HD 1438	–	–	–	<12.37	A-X (0,0)	<12.36	A-X
HD 1936	–	–	–	12.89 ± 0.18	A-X (0,0)	<12.17	A-X
HD 3240	–	–	–	<12.18	A-X (0,0)	<12.17	A-X
HD 3360	–	–	–	12.90 ± 0.27	A-X (0,0)	<12.08	A-X
HD 3369	–	–	–	<12.28	A-X (0,0)	<12.27	A-X
HD 3379	–	–	–	<12.37	A-X (0,0)	<12.36	A-X
HD 3901	–	–	–	12.74 ± 0.15	A-X (0,0)	12.22 ± 0.14	A-X
HD 5394	–	–	–	<12.00	A-X (0,0)	<12.00	A-X
HD 5550	–	–	–	<12.64	A-X (0,0)	<12.63	A-X
HD 6811	–	–	–	<12.12	A-X (0,0)	<12.11	A-X
HD 7636	–	–	–	13.53 ± 0.02	A-X (0,0)	12.97 ± 0.02	A-X

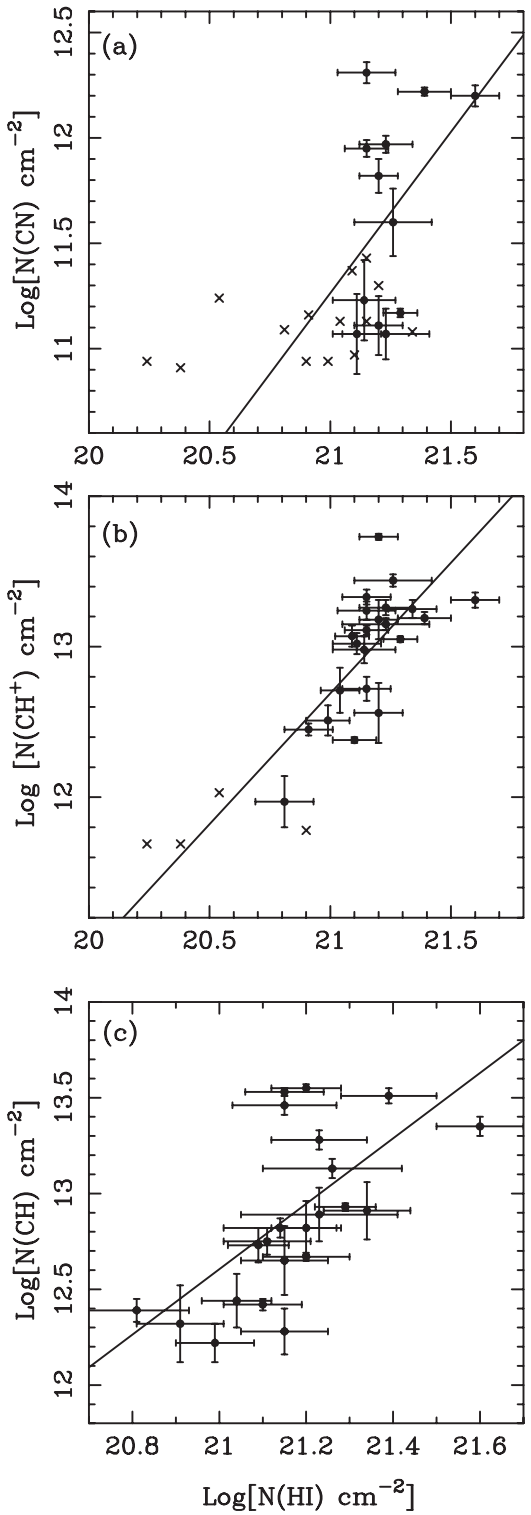

Figure 3. (a) Log of the CN (3873 Å) column density plotted against H I column density. (b) Corresponding plot for CH^+ (4232 Å). (c) Corresponding plot for CH (4300 Å).

is higher for CH^+ than for CN, implying that CH^+ is better mixed with H I than CN. Sheffer et al. (2008) find that when comparing *molecular* hydrogen column densities with those of CN, CH^+ or CH, the best fit is not a simple power law, but a twin-power-law relationship. The reason for this is postulated as being caused by different molecular gas chemical processes (equilibrium or non-equilibrium), depending on the density of the gas. The current data set comparing the *atomic* gas column densities with CN, CH^+ or CH is too scattered to show any such twin-power law.

4.2 Correlations between the column density of CN, CH^+, CH and Na I

Fig. 4 shows the correlations between the total column density of each of the three molecules studied, plus the Na I measurements taken from Paper I. The latter were derived using the lines at 3302 and 3303 Å, so are not subject to saturation problems as can be the case for Na I D. Fig. 5 shows the corresponding plots but on a component-by-component basis, where components separated by less than 2 km s^{-1} are assumed to be linked to the same parcel of gas.

4.2.1 CH versus CH^+

Early work by Crawford (1995) found that in most sightlines studied at low resolution, the vast majority that have a CH component also show CH^+ absorption. Further work by Gredel (1997) towards five open clusters also found a correlation between N(CH) and $N(CH^+)$, although the scatter is large. Gredel noted that part of the scatter is likely to be due to saturation effects, and partly if CH^+ is formed under turbulent conditions. More recent work by Pan et al. (2005) has suggested that there are two kinds of CH in diffuse molecular gas, being CN-like CH and CH^+-like CH. This appears to be due to the fact that CN is thought to probe the densest regions of clouds (e.g. Cardelli et al. 1990; Federman et al. 1994; Crawford 1995), CH intermediate densities, and CH^+ lower densities (cf. fig. 6 of Pan et al. 2005). Hence, sightlines with a lot of CN, in which the CH is associated with the CN, tend to show poor correlations between CH and CH^+ (e.g. Crane et al. 1995). By contrast, other more diffuse sightlines that show less CN have much stronger correlations between CH and CH^+ (e.g. Federman, Welty & Cardelli 1997). For the current data set, the total column density for all sightlines shows a reasonable correlation (correlation coefficient = 0.63) between CH and CH^+ as viewed in Fig. 4(d). From the work of Pan et al. (2005), this is to be expected, because as described in Bagnulo et al. (2003) and Paper I, both the entire POP data set and O- and B-type sample were not chosen specifically to probe molecular clouds.

We now consider component-by-component correlations as opposed to the correlations in the total values described above. For CH versus CH^+ for the components, Fig. 5 also demonstrates that for this data set the two molecules are reasonably well correlated, compared to the Pan et al. (2005). Pan et al. note that when all components are considered the correlation is weak, but much stronger when CH^+-like (as opposed to CN-like) components are fitted.

4.2.2 CN versus CH^+ and CH

Fig. 5 shows the CN column density plotted against that of CH and CH^+. Federman et al. (1994) find a good relationship between the total column density of CN and CH, with Pan et al. (2005) showing an even tighter one using a component-based approach. The current observations show a reasonable correlation. For CN against CH^+, the correlation is weaker, which is in line with the results in the previous sections.

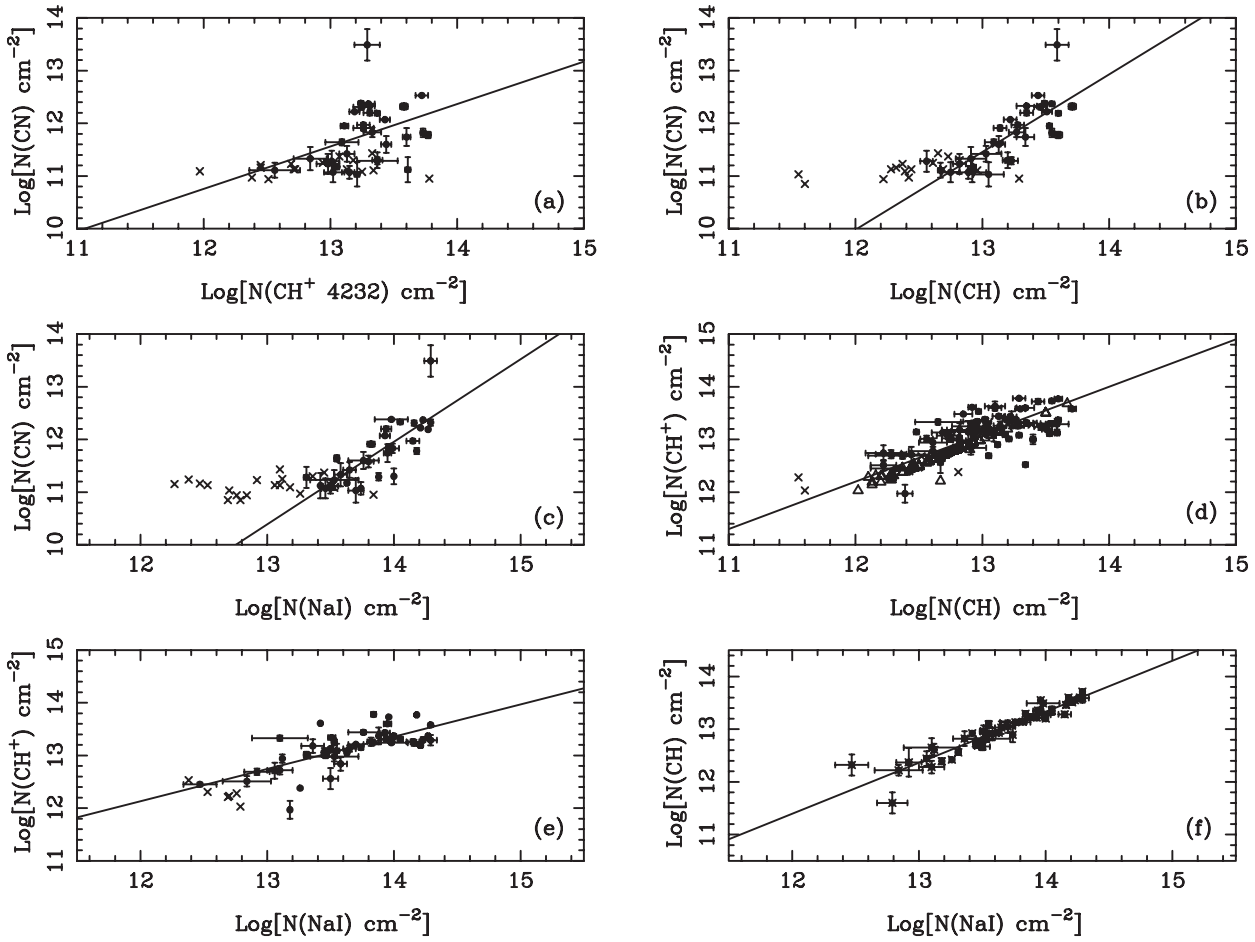

Figure 4. (a) Log of the CN (3874 Å) total column density plotted against log of the CH^+ (4232 Å) total column density obtained by summing all observed components. (b) Corresponding plot for CN (3874 Å) against CH (4300 Å). (c) Corresponding plot for CN (3874 Å) against Na I (3302 Å). (d) Corresponding plot for CH^+ (4232 Å) against CH (4300 Å). (e) Corresponding plot for CH^+ (4232 Å) against Na I (3302 Å)4. (f) Corresponding plot for CH (4300 Å) Na I (3302 Å). Filled circles are points with measurements, crosses with upper limits in the ordinate only and triangles with upper limits in both ordinate and abscissa.

4.2.3 CN, CH and CH^+ versus Na I

Concerning the total column densities, CN and CH^+ show reasonable correlation against Na I (measured using the UV lines at 3302 and 3303 Å, Figs 4c and e). The best correlation is found between CH and Na I (3302 Å, 3303 Å). This seems to confirm the work of Pan et al. (2005), who find that K I is well correlated with CH and generally co-exists, just as Na I generally co-exists with K I (e.g. Welty & Hobbs 2001; Smoker & Ledoux, in preparation, Paper V).

4.3 Correlations between the *b*-values of different molecules

In the data set of Welty, Morton & Hobbs (1996), high-resolution (0.3–1.2 km s^{-1}) spectra were used to provide important constraints on the physical conditions within clouds. In particular, the comparison of *b*-values between two species of different atomic weights (Ca II and Na I) were used to differentiate thermal and turbulent broadening. This is because the *b*-value is related to the mass (m), temperature (T) and turbulent velocity v_t, thus: $b = (2kT/m + v_t^2)$, where k is Boltzmann's constant. In particular, Welty et al. note that if Ca II and Na I D were similarly distributed, then $0.76 \leq b(\mathrm{Ca\,II})/b(\mathrm{Na\,I}) \leq 1.0$, with the lower and upper limits corresponding to purely thermal and turbulent broadening, respectively. On the other hand, a comparison of *b*-values for elements of similar atomic weights (e.g. Ca and K or to an extent Ti) can be used to directly determine whether a particular line studied samples the same part of the ISM. The current data set are of resolution 3.8 km s^{-1} ($b = 2.25$ km s^{-1}), and hence, it is likely that many *b*-values of less than ∼1.1 km s^{-1} are uncertain, and several of the features studied are likely to be blends. In particular, Crawford (1995) found median *b*-values for CN, CH and CH^+ of 0.63, 1.5 and 2.3 km s^{-1}, respectively. For the same molecules Pan et al. (2005) obtained $b = 0.83$, 1.04 and 1.96 km s^{-1}, respectively. These compare to the median *b*-values in the current data set of 1.3, 3.1 and 3.1 km s^{-1} for CN, CH^+ and CH, respectively, which are higher than the earlier work due to the lower resolution of the current data set. However, the CN *b*-values are clearly lower than for the other two molecules, as expected due to the higher atomic weight of the molecule and the fact that it appears to exist in higher density environments than either CH or CH^+.

4.4 The $^{12}CH^+/^{13}CH^+$ ratio

The ratio of $^{12}CH^+/^{13}CH^+$ is a tracer of stellar yields, in particular giving information concerning the relative importance of stars

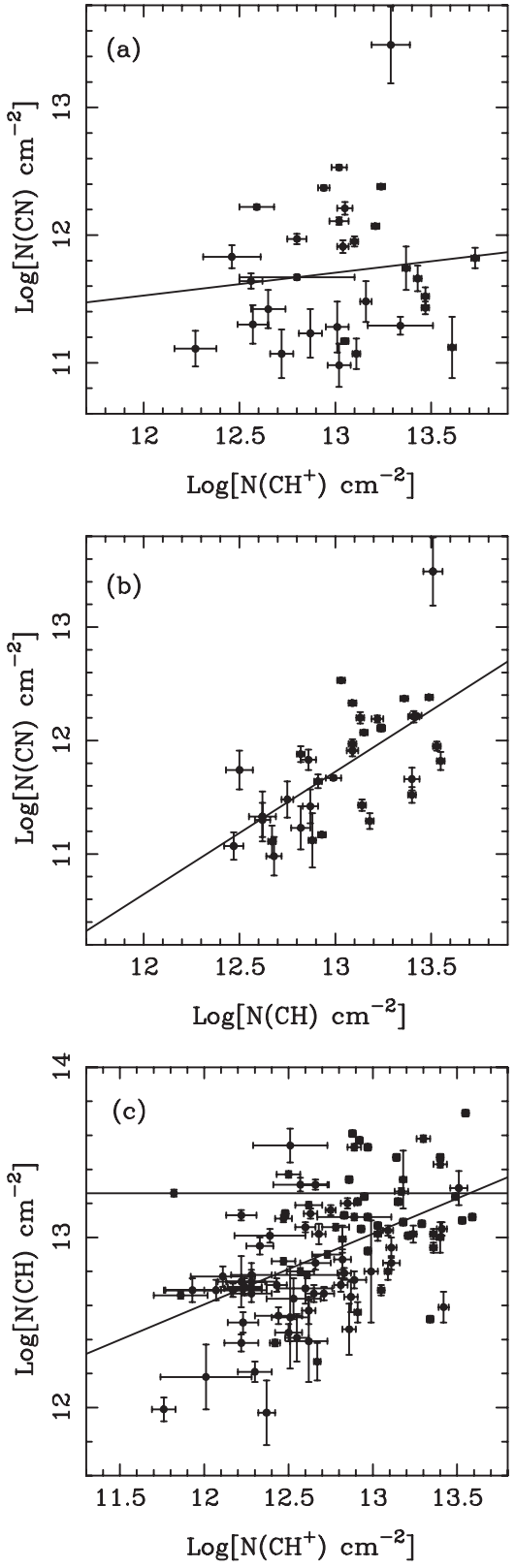

Figure 5. (a) Log of the CN (3874 Å) column density plotted against log of the CH^+ (4232 Å) column density for components which lie within 2 km s^{-1} of each other. (b) Corresponding plot for CN (3874 Å) against CH (4300 Å). (c) Corresponding plot for CH (4300 Å) against CH^+ (4232 Å).

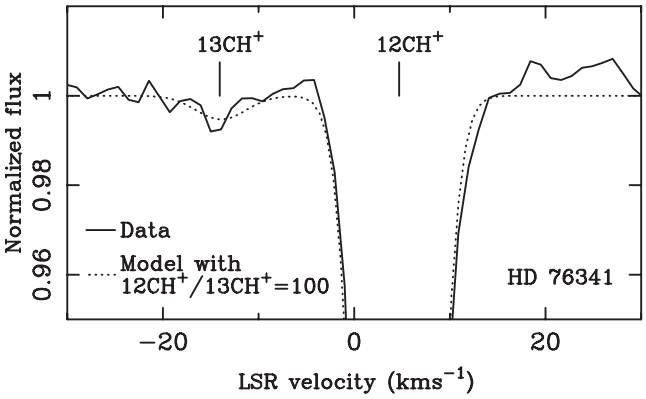

Figure 6. Solid line: normalized CH^+ (4232 Å) spectrum of HD 76341. Dashed line: model spectrum with the $^{13}CH^+$ component at –16.6 km s^{-1} given an abundance of 1 per cent of the $^{12}CH^+$ value at a spectral resolution of 80 000.

of different masses to the enrichment of the ISM (e.g. Vanden Bout & Snell 1981; Stahl, Casassus & Wilson 2008, and references therein). The $^{13}CH^+$ line lies 0.265 Å bluewards of the $^{12}CH^+$ line at 4232 Å and 0.44 Å *redwards* of the $^{12}CH^+$ line at 3957 Å, which can help in disentangling the effects of multiple components, if the intrinsic line width is narrow. Note that the spectral resolution of the current data is ∼0.06 Å, in theory sufficient to resolve the two species. Casassus, Stahl & Wilson (2005) found that within *local* interstellar clouds (i.e. closer than 100 pc) the observed isotopic ratio is from 62.2 ± 5.3 → 98.9 ± 10.1, demonstrating significant inhomogeneity in the local ISM and the need for high S/N ratio observations for the detection of $^{13}CH^+$. Similar results were obtained by Stahl et al. (2008) although the measurements are difficult and not in agreement with Ritchey et al. (2011), who find no evidence for variation of $^{12}CH^+/^{13}CH^+$ within 1 kpc of the Sun.

Inspection of the stars that show the strongest CH^+ absorption does not provide a firm detection for the $^{13}CH^+$ component, although the current data set does provide sightlines that could be observed at higher S/N ratio. One of these is HD 76341, in which the main component has a total column density in $\log[N(CH^+)\ \mathrm{cm}^{-2}] = 13.73$ and the spectrum has S/N ratio of ∼400 per pixel. The CH^+ 4232 Å profile is shown in Fig. 6 in which a model has been overlaid where the isotopic ratio has been set to 1 per cent. Possible absorption is seen in the $^{13}CH^+$ feature, but it is too close to the noise to be reliable. A spectrum with S/N ratio of ∼1000 would be easily attainable with UVES, and would provide an estimate of the isotope ratio for the line of sight to the star at a distance of ∼2.4 kpc (Paper I).

4.5 Comparison between the velocity centroids of CH and CH^+ and search for evidence of shocks

Pineau de Forêts et al. (1986) predicted that differences in the observed velocities of CH^+ and CH may indicate the presence of magnetic shocks, especially for high values of CH^+ column density. A shock with speed of ∼10 km s^{-1} may cause a temperature increase exceeding 1000 K (Gredel, van Dishoeck & Black 1993). Velocity offsets have been observed by Allen (1994) who found shifts on average of 2.6 km s^{-1} when comparing CH and CH^+ in the same sightline, although with low S/N ratios. Shifts of

$\sim$3 km s^{-1} were also found by Weselak et al. (2008a) for a few sightlines. However, velocity shifts were not found towards five OB associations studied by Gredel (1997) at a spectral resolution $R = 80\,000$, nor by Crawford (1995) at a resolution exceeding half a million. The current data have a spectral resolution of 80 000 or $\sim$3.8 km s^{-1}, allowing us to measure the centres of strong lines to an accuracy exceeding $\sim$1.5 km s^{-1} when we consider data with S/N ratios of several hundred. Inspection of the nine sightlines with absolute velocity difference of a component in CH and CH^+ greater than 1.5 km s^{-1} shows that the majority occur when there are low S/N ratio, and/or wide or blended components. The three sightlines with the most convincing difference in velocity between CH and CH^+ are present in HD 115363, HD 148937 and HD 151932. Even in these cases, the differences may well be caused by blends with the CH column density more closely following the CN column density as opposed to CH^+. We thus conclude that the current data set shows no evidence for shifts between CH and CH^+ of greater than $\sim$1.5 km s^{-1}, and hence no strong evidence for shocks.

5 SUMMARY AND FUTURE WORK

We have used data from the UVES POP Survey and other archive material to investigate the interstellar lines of CN (3874 Å), CH^+ (3957, 4232 Å) and CH (3886, 4300 Å), and compared the derived column densities with each other and also with a number of other measured parameters. CH is found to be very well correlated with Na I in the range $\log[N(\mathrm{Na\,I})\,\mathrm{cm}^{-2}]\sim$12.2–14.2. Although a number of cases with differences in CH and CH^+ velocity centroids have been identified, these appear to be caused by differences in strength between the components and not velocity offsets. Hence, in the current data set there are no clear cases of single-component sightlines showing large velocity shifts between CH and CH^+ that could have been caused by shocks. Finally, a search is undertaken for $^{13}CH^+$ in a sightline towards HD 76341 at an S/N ratio of 400 per pixel. No $^{13}CH^+$ is unambiguously detected, placing a limit on the $^{13}CH^+$ to $^{12}CH^+$ ratio of $\sim$0.01. A higher S/N spectrum towards this sightline would be interesting.

In a future paper, we will investigate the Routly–Spitzer effect (Routly & Spitzer 1952) of column density ratio versus LSR velocity for the neutral lines of Fe I (3719 Å), Ca I (4226 Å), Li I (6708 Å) and K I (7698 Å) which will be compared to the molecular lines discussed in the current paper and to Na I (UV), Ti II and Ca II taken from Paper I.

ACKNOWLEDGEMENTS

We would like to thank the staff of the Very Large Telescope, Paranal, for the work involved in producing the POP survey. ESO DDT programme ID 266.D-5655(A), http://www.sc.eso.org/uvespop. This research has made use of the SIMBAD data base, operated at CDS, Strasbourg, France. JVS is grateful to Queen's University Belfast and to the European Southern Observatory for funding under the auspices of the QUB visiting scientist fund and to ESO's Director General Discretionary Fund which supported this work. Finally, we are very grateful to the extensive comments and corrections provided by the anonymous referee which greatly improved the paper.

REFERENCES

Allen M. M., 1994, ApJ, 424, 754
Bagnulo S., Jehin E., Ledoux C., Cabanac R., Melo C., Gilmozzi R., 2003, ESO Messenger, 114, 10
Cardelli J. A., Edgar R. J., Savage B. D., Suntzeff N. B., 1990, ApJ, 362, 551
Casassus S., Stahl O., Wilson T. L., 2005, A&A, 441, 181
Crane P., Lambert D. L., Sheffer Y., 1995, ApJS, 99, 107
Crawford I. A., 1995, MNRAS, 277, 458
Dekker H., D'Odorico S., Kaufer A., Delabre B., Kotzlowski H., 2000, Proc. SPIE, 4008, 534
Falgarone E., Phillips T. G., Pearson J. C., 2005, ApJ, 634, 149
Federman S. R., 1982, ApJ, 253, 601
Federman S. R., Danks A., Lambert D., 1984, ApJ, 287, 219
Federman S. R., Strom C. J., Lambert D. L., Cardelli J. A., Smith V. V., Joseph C. L., 1994, ApJ, 424, 772
Federman S. R., Welty D. E., Cardelli J. A., 1997, ApJ, 481, 795
Gredel R., 1997, A&A, 320, 929
Gredel R., van Dishoeck E. F., Black J. H., 1991, A&A, 251, 625
Gredel R., van Dishoeck E. F., Black J. H., 1993, A&A, 269, 477
Howarth I. D., Price R. J., Crawford I. A., Hawkins I., 2002, MNRAS, 335, 267
Howarth I. D., Murray J., Mills D., Berry D. S., 2003, Starlink User Note SUN 50. Rutherford Appleton Laboratory/CCLRC, Oxfordshire
Hunter I., Smoker J. V., Keenan F. P., Ledoux C., Jehin E., Cabanac R., Melo C., Bagnulo S., 2006, MNRAS, 367, 1478 (Paper I)
Kaufer A., Wolf B., Andersen J., Pasquini L., 1997, The Messenger, 89, 1
Lambert D. L., Sheffer Y., Crane P., 1990, ApJ, 359, 19
Lavalley M. P., Isobe T., Feigelson E. D., BAAS, 24, 839
Lien D. J., 1984, ApJ, 284, 578
Mooney C. J., Rolleston W. R. J., Keenan F. P., Dufton P. L., Smoker J. V., Ryans R. S. I., Aller L. H., 2002, MNRAS, 337, 851
Mooney C. J., Rolleston W. R. J., Keenan F. P., Dufton P. L., Smoker J. V., Ryans R. S. I., Aller L. H., Trundle C., 2004, MNRAS, 419, 1123
Moultaka J., Ilovaisky S. A., Prugniel P., Soubiran C., 2004, PASP, 116, 821
Pan K., Federman S. R., Cunha K., Smith V. V., Welty D. E., 2004, ApJS, 151, 313
Pan K., Federman S. R., Sheffer Y., Andersson B.-G., 2005, ApJ, 633, 986
Pineau de Forêts G., Flower D. R., Hartquist T. W., Dalgarno A., 1986, MNRAS, 220, 801
Ritchey A. M., Federman S. R., Lambert D. L., 2011, ApJ, 728, 36
Routly P. M., Spitzer L., 1952, ApJ, 115, 227
Sahu M. S., Blades J. C., He L., Hartmann D., Barlow M. J., Crawford I. A., 1998, ApJ, 504, 522
Sheffer Y., Rogers M., Federman S. R., Abel N. P., Gredel R., Lambert D. L., Shaw G., 2008, ApJ, 687, 1075
Slyk K., Bondar A. V., Galazutdinov G. A., Krelowski J., 2008, MNRAS, 390, 1733
Smoker J. V., Haffner L. M., Jeenan F. P., Davies R. D., Pollacco D., 2002, MNRAS, 337, 385
Smoker J. V. et al., 2003, MNRAS, 346, 119
Smoker J. V. et al., 2007, MNRAS, 378, 947 (Paper II)
Smoker J. V. et al., 2009, ESO Messenger, 138, 8
Smoker J. V., Bagnulo S., Cabanac R., Keenan F. P., Fossati L., Ledoux C., Jehin E., Melo C., 2011, MNRAS, 414, 59 (Paper III)
Stahl O., Casassus S., Wilson T., 2008, A&A, 477, 865
Vanden Bout P. A., Snell R. L., 1981, ApJ, 246, 1045
Wallace P., Clayton C., 1996, RV, Starlink User Note SUN 78. Rutherford Appleton Laboratory/CCLRC, Oxfordshire
Welty D. E., Hobbs L. M., 2001, ApJS, 133, 345
Welty D. E., Hobbs L. M., Penprase B. E., Blitz L., 1989, ApJ, 346, 232
Welty D. E., Morton D. C., Hobbs L. M., 1996, ApJS, 106, 533
Welty D. E., Federman S. R., Gredel R., Thorburn J. A., Lambert D. L., 2006, ApJS, 165, 138

Weselak T., Galazutdinov G., Musaev F., Krelowski J., 2008a, A&A, 479, 149
Weselak T., Galazutdinov G. A., Musaev F. A., Krelowski J., 2008b, A&A, 484, 381
Weselak T., Galazutdinov G. A., Musaev F. A., Beletsky Y., Krelowski J., 2009, A&A, 495, 189

SUPPORTING INFORMATION

Additional Supporting Information may be found in the online version of this article:

Appendix A: Online material
(http://mnras.oxfordjournals.org/lookup/suppl/doi:10.1093/mnras/stt2261/-/DC1).

Please note: Oxford University Press are not responsible for the content or functionality of any supporting materials supplied by the authors. Any queries (other than missing material) should be directed to the corresponding author for the article.

This paper has been typeset from a TEX/LATEX file prepared by the author.